electronics

MDPI

Article

A Real-Time Scheduling Approach to Mitigation of Li-Ion Battery Aging in Low Earth Orbit Satellite Systems

Seongik Jang and Hoeseok Yang *

Department of Electrical and Computer Engineering, Ajou University, 206 Worldcup-ro, Yeongtong-gu, Suwon-si 16499, Korea; vital5968@ajou.ac.kr

* Correspondence: hyang@ajou.ac.kr; Tel.: +82-32-219-2361

Abstract: Thanks to their higher performance compared to conventional batteries, lithium-ion (Li-ion) batteries have recently become popular as a power source in many electronic systems. However, Li-ion batteries are known to suffer from an aging issue: the available capacity is gradually degraded as the operation goes by. The impact of aging is particularly critical to satellite systems where no maintenance is available after the initial deployment. Recently, a real-time scheduling framework was proposed to decelerate the aging of Li-ion batteries. However, this framework simply relies on the fact that the elevated temperature results in a worse lifespan of the battery. In contrast to this, in this paper, we argue that the reduced temperature may actually cause an adverse effect in the battery lifetime when considering satellite environments. To evidently demonstrate this anomaly, we extend an open-source Li-ion battery aging simulator to consider the temperature-dependent aging characteristics of the Li-ion batteries. Then, a couple of alternative scheduling policies that better suit the target satellite systems are evaluated in the simulator in comparison with the existing scheduling policies. Our simulation results show that the existing scheduling method, which does not consider the satellite temperature environments, rather deteriorates the lifespan of battery and the proposed scheduling technique can extend the lifespan by up to 65.51%.

Keywords: real-time embedded systems; lithium-ion battery aging; lifespan; low earth orbit satellites

Citation: Jang, S.; Yang, H. A Real-Time Scheduling Approach to Mitigation of Li-Ion Battery Aging in Low Earth Orbit Satellite Systems. *Electronics* **2021**, *10*, 86. https://doi.org/10.3390/electronics10010086

Received: 19 November 2020
Accepted: 28 December 2020
Published: 4 January 2021

1. Introduction

Lithium-ion (Li-ion) batteries have been popularly used as a power source in mobile devices thanks to their longer lifespan and higher energy density than conventional batteries [1]. Their popularity is not only limited to customer electronics, but also increasingly attracting attention in other real-time systems such as Electric Vehicles (EVs), Unmanned Aerial Vehicles (UAVs) and satellites.

However, the Li-ion batteries suffer from some limitations such as safety, non-linear performance, and aging issues. In particular, the battery aging issue is directly related to the lifetime of a system when physical maintenance is infeasible, which is the main challenge of this paper. The battery aging is usually represented by a capacity degradation which is caused by a huge number of repeated cycles of charging and discharging. It is common for electronic devices to become unusable due to this battery aging, instead of due to failure of electronic or mechanical parts. In other words, the lifespan of a battery has become a main bottleneck of the lifetime in battery-powered systems.

This aging effect has different impacts depending on the characteristics of systems. While the impact of aging only causes some inconveniences in mobile devices, the same level of aging would result in more critical consequences in other domains. In the case of an EV which is equipped with a large number of batteries, the battery replacement cost due to aging may be excessive. Moreover, a deteriorated health of battery sometimes makes system operation unpredictable which can lead to catastrophic consequences in safety-critical systems.

Among various systems, the impact of aging is particularly fatal to satellite systems where no maintenance is available after the initial deployment. Since Low Earth Orbit (LEO) satellites revolve around the Earth, the sunlight period, in which the system is exposed to sunlight, and the eclipse period, in which the Sun is blocked by the Earth, repeatedly appear in an interleaved way. Note that harvesting energy from solar panels in the satellite is only available during the sunlight period. Thus, during the energy-constrained eclipse period, the battery is the only power source of the entire system. This implies that the lifespan of satellite systems, which cost a lot for launch, can be compromised by the aging of the batteries.

There are a handful of works that mitigate the aging of batteries for the satellite systems. For a longer battery lifespan, Maheshwari et al. [2] proposed a transmission power control technique that distributes traffic between adjacent satellites on the same orbit plane. This study utilized the fact that the smaller amount of the required charge per cycle, i.e., the shallower the depth of discharge (DOD), the longer the expected battery lifespan. In addition to the DOD minimization, Lami et al. [3] claimed that minimizing the state of charge (SOC) swing, i.e., the range of the used capacity, can extend the battery lifespan. However, the above works have simply estimated the lifespan as a function of DOD and this modeling is only valid under a narrow condition where the data for modeling was obtained or measured. How the highly varying temperature condition of the satellite systems would affect the battery lifetime has not been investigated in their studies.

There have been some studies in other industrial domains to mitigate the aging of the Li-ion battery. Chon et al. [4] proposed a battery use guide scheme, targeting the smartphone domain, that is based on a large-scale use-case profiling with crowdsensing. Wegmann et al. [5] investigated the aging of hybrid battery with two different cell types and reported that proper load splits between different cell types could improve the battery lifetime at long recuperation phases in EV. However, none of these works can be directly applied to satellite systems due to the heterogeneity in workload and the lack of large-scale profiling data.

Recently, Kwak et al. [6] proposed a real-time scheduling framework, called Reserved Execution Time (RET),that tries to maximize the battery lifetime in UAV systems. Based on a Li-ion battery aging model proposed by [7], they tried to reduce the internal heat dissipation out of battery to mitigate the aging factors. While they did consider the effects of temperature in the battery aging, they basically assumed that the elevated temperature always results in a worse battery lifetime. This does not always hold true even for the systems operating on the Earth [8]. Furthermore, this assumption is increasingly unrealistic when considering radical temperature changes often observed in the satellite systems. Indeed, there have been several works that demonstrated low temperatures could also cause adverse effects on battery aging [9,10]. Wu et al. [11] also investigated battery aging of a number of batteries cycles with different discharge profiles at low temperature and showed that the aging can be mitigated by increasing the battery temperature. However, they did not propose any specific method how to increase the battery temperature. This work focuses on how a real-time task scheduling approach can mitigate this adverse effect within the given timing and power budget imposed in the satellite systems.

In this regard, we argue that the existing scheduling policy [6] that was proposed to lengthen the battery lifetime may actually cause the opposite result for the satellite systems. To evidently demonstrate this anomaly, we evaluate the lifetimes of batteries used for satellite system on top of an open-source Li-ion battery aging simulator [12]. In doing so, we first model the hardware and software behaviors of the target LEO satellites and their ambient temperature changes throughout the revolution period in Section 2. Section 3 reviews a number of aging factors of Li-ion batteries that have been considered or ignored in the existing techniques and how they can be affected by temperature changes. Based on the discussed aging factors, we propose a modified scheduling policy that suits better to the satellite systems in Section 4. It is shown in Section 5 that the proposed technique

outperforms the existing technique in terms of the expected lifetime of Li-ion battery in satellite systems, followed by concluding remarks in Section 6.

2. System Model

In this section, we describe how we model the satellite systems, their workloads (tasks), and their working environments to quantitatively evaluate the battery aging.

2.1. Models for Target Satellite Systems and Their Workloads

The LEO satellites that we target in this paper refer to the satellites orbiting the Earth at a low altitude (<2000 km) [13]. These LEO satellites are generally powered by the energy harvested from solar panels, which charges the battery when exposed to sunlight. During the eclipse period, the satellite system solely relies on the battery. For simplicity, we model the system with a single battery pack without loss of generality. Furthermore, we consider no overcharge/discharge, which is known to cause irreversible damage [14,15], or cell balancing problems, which may result in sub-optimal energy efficiency in multi-cell batteries [16], as the underlying battery management system is assumed to evenly distribute the current demands in an optimal way.

A satellite system S consists of n subsystems (A subsystem can be any of hardware/software components that may independently demand power dissipation, e.g., sensor modules, communication modules, processors, and so forth), i.e., $S = \{S^1, S^2, ..., S^n\}$. A subsystem S^j executes a set of its own power-consuming real-time tasks $\tau^j = \{\tau_1^j, \tau_2^j, ..., \tau_k^j\}$ which are executed mutually exclusively in a subsystem. That is, a subsystem can execute only one task at a time. Each task $\tau_i^j \in \tau^j$ is characterized by a tuple of three constant parameters (T_i^j, X_i^j, P_i^j) that denote a minimum interval between successive execution requests, worst-case execution time (WCET), and a constant current consumption. As each task is characterized with these three constant values, we can uniquely identify the current discharging behavior of the system as a single representative current trace once the starting time of each task is fixed. It is worthwhile to mention that this workload model is a widely accepted one as in other battery-aware scheduling techniques [6]. We also assume that the minimum scheduling time unit is as small as 10 ms and the period/WCET are represented as an integer number that is a multiple of minimum time unit. We consider sporadic/periodic non-preemptive tasks with implicit deadline, i.e., the tasks should be completed before the next execution request and a task execution is indivisible, thus cannot be interfered by other tasks in the same subsystem.

Under these assumptions, the system model can be converted to a partitioned scheduling on multi-core processors where each subsystem is abstracted as a processor executing its own pre-assigned real-time power-consuming tasks. Note that, in the target problem, the task-to-processor, i.e., task-to-subsystem, assignment is given by the design of the satellite system. We only decide on when each subsystem (processor) executes the tasks in order to minimize a battery aging while respecting all real-time constraints.

2.2. LEO Satellite Orbit Operation and Ambient Temperature Model

LEO satellites generally have different revolution periods depending on missions. In this paper, we assume that the the target system has a revolution period of 100 min consisting of 38 min of eclipse period and 62 min of sunlight period as exemplified in [17]. The batteries in the target system are being discharged only during the eclipse period, while generation and consumption of energy happen at the same time during the sunlight period. That is, within the sunlight period, the batteries are charged as much as the surplus power, i.e., harvested power by solar panels subtracted by the consumed amount by all subsystems. However, if eventually the harvested power is not enough for the power demand, the batteries can also be discharged; that is, if more current is required than the solar panel generates, the batteries would be discharged. In other words, the batteries could also be discharged during the sunlight period as Mostacciuolo et al. [18,19] showed in their work.

The revolution behavior of the LEO satellite results in regular and predictable temperature changes; Exposure to the sunlight heats up the system temperature during the sunlight period. Conversely, it cools down during the eclipse period. As a result, satellites orbiting around the Earth, experience extremely varying ambient temperature depending on a presence or absence of sunlight. This behavior is also confirmed in other small satellite systems [20]. As the ambient temperature is different depending on the architecture or configuration of designed satellite, we borrow the ambient temperature model from the work of Lee et al. [17] which is illustrated in Figure 1. They assume the ambient temperature varies linearly within [0 °C, 30 °C) for which the eclipse period (between $t = 0$ and $t = 38$) and the sunlight period (between $t = 38$ and $t = 100$) last. This can be formulated as follows:

$$T_{ambient}(t) = \begin{cases} 30 - \frac{38}{30}t, & \text{if } 0 \leq t < 38 \\ \frac{30}{62}(t - 38), & \text{if } 38 \leq t < 100 \end{cases} \quad (1)$$

where t denotes the relative time in the unit of minutes within a 100-min of revolution period.

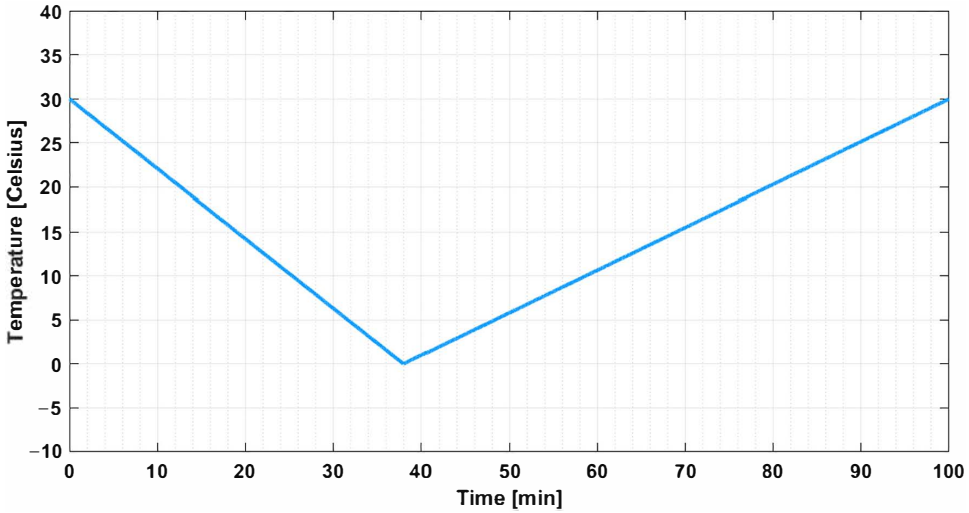

Figure 1. An ambient temperature model with one orbit period [17].

3. Li-Ion Battery Aging Model for Satellite Systems

In this section, we review the Li-ion battery aging models with two common aging factors (Solid Electrolyte Interface and active material loss), which are widely adopted in estimating the battery lifetime. Then, we extend the model to be accurately used for satellite systems that operate in highly varying ambient temperatures by considering the lithium plating effect.

3.1. Li-Ion Battery Degradation Model

Li-ion battery degradation models that are used for battery lifespan estimations can be categorized into two: empirical model [21,22] or electro-chemical model [23–25]. The empirical ones are not based on the sophisticated modeling of underlying physical processes, but merely rely on the parameter fittings out of extensively measured battery cycling data [22]. While these empirical models offer a simple yet effective solution to the estimation of the battery lifetime, they only provide a limited analytic insight [26] and, more importantly, their applications are limited to the similar environments or conditions where the fitting data were obtained from. On the contrary, the electro-chemical model quantitatively characterizes the physical processes of internal battery behaviors [12]. Thus, this model can be applied to a wider range of operating conditions including the one that is not accessible at design-time, for instance, the space environment for satellite systems. We adopt an electro-chemical model in this work.

Kwak et al. [6] also used an electro-chemical model for the lifetime estimation of Li-ion batteries, based on two aging factors: Solid Electrolyte Interface (SEI) growth and active material loss. SEI refers to a compound layer which is formed as a result of a side reaction. That is, when lithium ions do not participate in the main reaction as depicted in Figure 2a, i.e., charging/discharging, for any reason, but are involved in unintended side reactions, a solid layer is accumulated either at the Anode or at the Cathode side as illustrated in Figure 2b. The other factor is the active material loss, which is gradually caused by mechanical stress induced by volume and structure changes [27]. Since Li-ion battery produces current by means of the movements of lithium ions, the loss of lithium ions that participate in the main reaction directly indicates a reduced battery capacity [28].

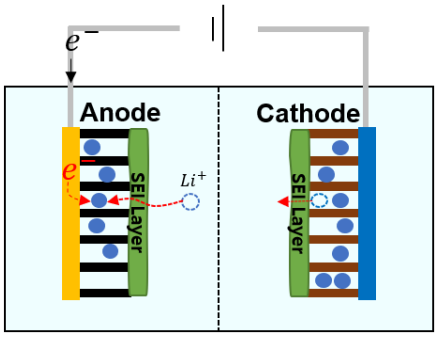

(**a**) A main reaction

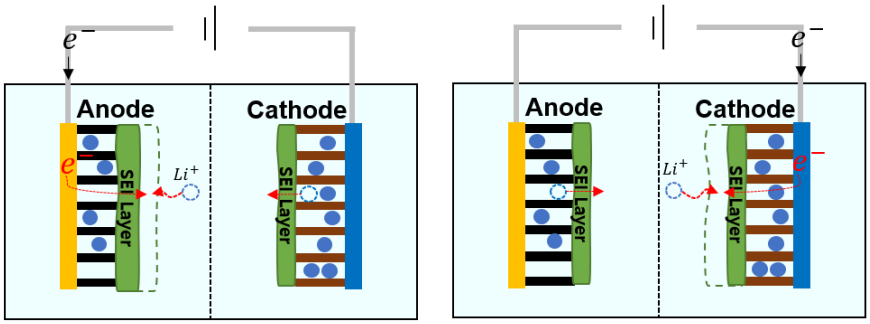

(**b**) Side reactions

Figure 2. The difference with main reaction and side reaction.

The both degradation effects stated above are known as to be accelerated in an elevated temperature. Jin et al. [23] modeled those two as functions of temperature, current, and SOC, based on which the battery capacity loss is quantitatively modeled.

3.2. Battery Temperature Model

As shown before, in order to accurately quantify the aging effects, it is necessary to model the temperature of the battery cell. Once the battery heating behaviors are characterized by the heat generation q_{gen} and the heat convection q_{conv}, the battery cell temperature T at time t can be formulated as follows:

$$\rho \cdot c_p \cdot \frac{dT(t)}{dt} = q_{gen} + q_{conv}, \tag{2}$$

where ρ and c_p are the density and heat capacity of battery, respectively.

The heat generation q_{gen} is attributed to four heat sources. Among these heat sources, the Joule ohmic heat is known to be the most significant factor of heat generation [29] and can be formulated as

$$q_{jou} = I^2 \cdot R \tag{3}$$

with I being the charged/discharged current and R being the effective DC resistance of the battery.

3.3. Lithium Plating Effect

Note that we target the battery in LEO satellite systems that operate in highly varying temperature environments as shown in Figure 1. In such cases, the battery aging model should be properly extended considering the radical changes in the ambient temperature. Existing battery aging models, e.g., the one used by Kwak et al. [6], failed to take this into consideration. Specifically, they have not considered the lithium plating effect that can accelerate the aging when operating in a very low temperature.

The lithium plating is observed when the battery is charged at a low temperature [30]. In a normal charging process, lithium ions intercalate into anode as depicted in the Figure 3a. However, if the battery temperature is considerably low, diffusion at the anode side is slowed down resulting in the accumulated lithium ions at the surface of anode, as illustrated in the Figure 3b. This, in turn, causes the reduction of available lithium ions, and thus the capacity of the battery. Furthermore, it can also result in a dangerous consequence when the plated lithium induces an internal short circuit.

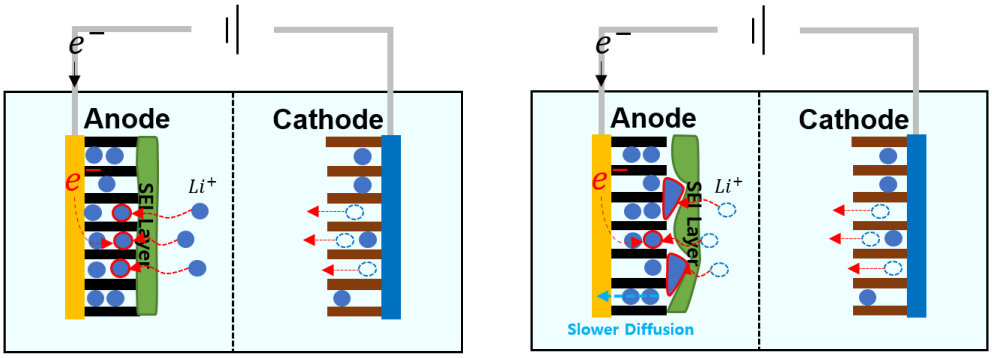

(**a**) Normal charging process (**b**) Lithium plating process

Figure 3. Charging processes in two conditions. (**a**) normal charging process without lithium plating effect; (**b**) charging process with lithium plating effect due to a slower diffusion in a low temperature.

It is worthwhile to mention that each of the aging factors stated above may be affected by the battery temperature in a different way. Typically, most chemical reactions, including SEI, are accelerated at a higher temperature [31]. However, it has been reported by Waldmann et al. [32] that the battery lifetime was the longest at 25 °C due to the adverse effect caused by the lithium plating effect at lower temperatures (<25 °C). In other words, the dominant factor that becomes the lifetime bottleneck may be different from one operating temperature to another. In this sense, Yang and Wang [8] investigated to figure out optimal temperature for lifespan of batteries and reported that the optimal temperature may vary depending on the cell characteristics as both the SEI growth and lithium plating effect should be considered at the same time. These suggest that it is important to manage the battery usage in a temperature-aware manner to prolong the battery lifetime in satellite systems that operate in highly varying temperature conditions.

4. Proposed Scheduling Method

In this section, we propose a new scheduling policy that maximizes the expected lifespan of Li-ion battery that is used in the target system modeled in Section 2. Kwak et al. [6] proposed a scheduling policy, called RET, to maximize the battery lifespan for real-time systems. They assumed a fixed normal ambient temperature which is usually about 300 K and did not take the lithium plating effect into consideration in estimating the battery lifetime. Therefore, in their modeling, it is always best to keep the temperature as low as possible. So, they proposed to minimize the heat dissipated by the battery, specifically q_{jou}

which is known as the most dominant factor in Equation (3) by scheduling. Given the workloads of the target system fixed, the sum of discharged currents from all subsystems remains unchanged for any scheduling decision (As no dynamic voltage or frequency scaling techniques considered, the amount of power (current) dissipated by all tasks is constant for different scheduling results.). Based on the thermal dynamics modeled in [6], it was proven that reducing the sum of squared currents by consumed by all tasks results in lesser heat generation. In other words, they tried to minimize the variance of current dissipation over time in the scheduling decision in order to maximize the battery lifetime.

However, such evenly distributed current dissipation loads may not always result in an extended expected battery lifetime for satellite systems. As elaborated in the previous section, they operate in highly varying temperature environments and the ambient temperatures mostly stay lower than the typical optimal temperature derived by Waldmann et al. [32], where the lithium plating effect may play a critical role in battery lifetime. In particular, it is expected that the battery temperature continuously decreases during the eclipse period. Charging Li-ion battery at low temperatures, e.g., right after the eclipse period, may accelerate the lithium plating effect [32].

As will be shown in the evaluations, if the lithium plating effect is additionally considered in the lifetime estimation, the reduced battery cell temperature caused by the RET scheduling policy results in rather shortened battery lifetime. Based on the observation of this anomaly, we propose an alternative battery-aware scheduling policy which better suits to the LEO satellite systems. It is hard to find out a single optimal operating temperature since it may vary from one battery characteristic to another [8]. Even if the optimal temperature point is known, it is not trivial to keep the battery cell temperature at the optimal point with respect to a set of heterogeneous workloads and the varying ambient temperatures. Note in Figure 1 that the satellite ambient temperature is mostly below than the normal room temperature (300 K) that normal systems operated on the Earth have. In this case, the lithium plating effect is alleviated in a higher temperature [8]. Therefore, in this work, we simply take the opposite approach to the RET framework; we try to place the current discharge loads as unbalanced as possible with respect to the real-time constraints in favor of increased temperature.

It is worth mentioning that, in this work, we restrict ourselves to the scope of scheduling in heating up the battery cell, which means the total amount of discharged current remains the same regardless of the scheduling decision. In the case that the harvested energy is sufficient to power all subsystems and charge the battery for a certain amount of time during the sunlight period, external thermal management techniques [33,34], e.g., using heaters, could be applied taking advantage of the extra power (current) to heat up the battery. However, due to the additional weight and manufacturing costs, it is not common to adopt such external thermal management approaches for small satellites [35]. Note that the proposed scheduling approach can be applied independently together with these external thermal management techniques. In this case, when and how much to actively heat up could be considered as yet another problem to be optimized with respect to the power availability.

Similarly to the RET framework [6], the proposed scheduling takes three-step off-/on-line hybrid approach. First, as an off-line procedure, it calculates virtual execution times, called reservation times (RV), for all tasks. These reservation times are assigned in a way that the reservation time of each task is maximized but never causes a deadline violation. Then, at run time, as a second step, it chooses a task to be scheduled next using a conventional real-time scheduling policy, e.g., Earliest Deadline First (EDF). If task τ_i is chosen for a subsystem in this step at time t, this task is said to be reserved for the subsystem at time t and the time range $[t, t + RV_i]$ is occupied by τ_i, i.e., no other tasks can be executed in this range.Finally, for a reserved task, when this task is executed should be fixed at run time within its reserved time range. That is, in the previous example, the actual starting time should be in the range $[t, t + RV_i - X_i)$.

4.1. Off-Line Calculation of Reservation Time (Common for the RET Framework and the Proposed Policies)

Algorithm 1 delineates the off-line calculation procedure of reservation times that the proposed algorithm and the RET framework [6] have in common. For each subsystem (processor), the reservation times of the tasks are initialized to their WCETs and all tasks are stored in Q in a descending order of current consumption (lines 2–3). Then, for each task popped from the head of Q, the reservation time is increased by 1 time quantum (line 6) and the schedulability is checked with this increased reservation time being the WCET (line 7). Once successful, this task is queued again into the tail of Q (line 8) and this procedure is repeated until there is no further room for the increment in reservation time in all tasks (lines 4–12). The idea is to find the largest time range of the task execution time that guarantees the real-time schedulability even in the unluckiest case, i.e., $WCET_u^w = RV_u^w$. For the schedulability analysis, the uni-core Non-Preemptive Earliest Deadline First (NP-EDF) scheduling condition dervied by Jeffay et al. [36] is used. This off-line scheduling algorithm takes a time complexity of $O(\max_{\tau_i^j \in \tau^j}(T_i^j - X_i^j) \cdot sched\_check(\tau^j))$ for subsystem S^j. Note that this reservation time calculation procedure is performed off-line, thus has no impact on the runtime behavior of the system.

Algorithm 1 Calculation of reservation times

1: **for** every $S^w \in S$ **do**
2: $Q \leftarrow \phi$; ▷ Initialized as an empty FIFO queue
3: $\forall \tau_u^w \in \tau^w$, initialize $RV_u^w \leftarrow X_u^w$ and enqueue them into Q in a descending order of P_u^w;
4: **while** $Q \neq \phi$ **do**
5: $\tau_u^w \leftarrow dequeue(Q)$;
6: $RV_u^w \leftarrow RV_u^w + 1$;
7: **if** $sched\_check(\tau^w) == schedulable$ with $X_u^w \leftarrow RV_u^w$ **then**
8: $enqueue(\tau_u^w)$ into the tail of Q;
9: **else**
10: $RV_u^w \leftarrow RV_u^w - 1$;
11: **end if**
12: **end while**
13: **end for**

4.2. On-Line Scheduling in RET

At run time, firstly, it should be decided which task is reserved using an ordinary scheduling policy. We call this default scheduling decision and used an EDF scheduler for this. Then, for each of the reserved ones, when to start its actual execution is judiciously determined within the reserved time range in a way that the variation of current dissipation over time is minimized during the precise scheduling in the RET framework. Being an on-line procedure, it is computationally intractable to investigate all possible scheduling cases when making this decision. Instead, it is decided by a heuristic algorithm illustrated in Algorithm 2 whenever a new task reservation occurs.

The procedure is given the current time stamp (t_{now}) and the array of the sum of the currents dissipated by subsystems at each time step ($I[t]$) for $[t_{now}, t_{max}]$ as input (lines 1–2) where t_{max} denotes the biggest time stamp at which actual scheduling decision is made among all subsystems. If a task is newly reserved by the default scheduling (line 3), all tasks that are reserved but not yet fixed in scheduling are enqueued into a tail of the Q in

a descending order of power consumption (lines 5–10). Note that a task that has already been fixed its execution time before should also be enqueued if it is yet to be in actual execution, i.e., t_{now} is smaller than its given starting time. Then, for each enqueued task, a feasible starting time within its reserved time range, i.e., $m \in [t_{now}, t_{now} + RV_u^w - X_u^w)$ such that the interval sum of system-wide current consumption is minimized, is searched (lines 14–19). Once found, the task is decided to be executed from that time on and the current (power) dissipation trace, $I[t]$ is updated as per the scheduling decision (lines 20–22). Note also that, if the actual task execution is completed than the end reserved time range, this reserved time should not be used for other tasks' executions.

Algorithm 2 Run time scheduling of the reserved tasks in the RET framework [6]

1: t_{now}: the current time step index
2: $I[t]$: current dissipation trace for $t \in [t_{now}, t_{max}]$
3: **if** a new task is reserved **then** ▷ By the default scheduling decision
4: $Q \leftarrow \phi$; ▷ Initialized as an empty queue
5: **for** each $S^w \in S$ **do**
6: **if** S^w is reserved by τ_u^w and not in execution **then**
7: $enqueue(\tau_u^w)$ into Q;
8: **end if**
9: **end for**
10: Sort Q in a descending order of P_u^w; ▷ From more power-consuming ones to lesser
11: **while** $Q \neq \phi$ **do**
12: $\tau_u^w \leftarrow dequeue(Q)$;
13: $min \leftarrow \infty$; $start \leftarrow t_{now}$;
14: **for** m in [t_{now}, t_{now}+$RV_u^w - X_u^w$) **do**
15: $temp \leftarrow \sum_{t=m}^{m+X_u^w-1} \{I[t] + P_u^w\}$;
16: **if** $temp < min$ **then**
17: $min \leftarrow temp$; $start \leftarrow m$;
18: **end if**
19: **end for**
20: **for** $i \in [start, start + X_u^w)$ **do** ▷ Update $I[t]$ as per the decided starting time of τ_u^w
21: $I[i] \leftarrow I[i] + P_u^w$;
22: **end for**
23: **end while**
24: **end if**

Figure 4 illustrates scheduling examples from the EDF and RET policies in comparison. In the EDF policy, the scheduling decision is made in a work-conserving manner, i.e., no task is allowed to defer its execution when the processor is idle. Thus, in subsystem S^i, τ_a^i and τ_b^i are executed back-to-back without any slack in-between at the beginning. On the contrary, the RET framework first assigns the reservation time ranges for the two tasks and separate them in time within their own reservation time ranges, resulting in the total current dissipation workloads are more evenly distributed. For instance, by the RET policy, τ_a^i in S^i is discouraged to be overlapped with other tasks in other subsystems and that is

why τ_a^j and τ_b^j are separately executed in S^j and τ_a^i is scheduled in the slack caused by these two tasks.

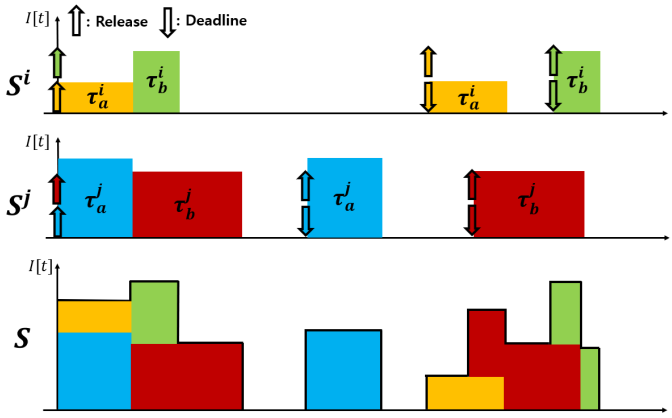

(**a**) A general Earliest Deadline First (EDF) scheduling example

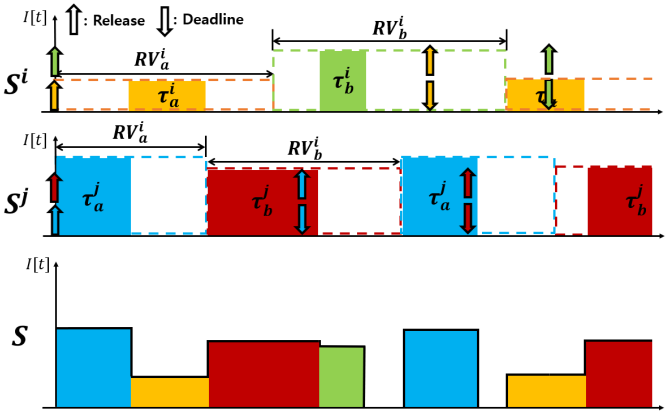

(**b**) A scheduling example from the Reserved Execution Time (RET) policy

Figure 4. Examples of scheduling and current dissipation traces from (**a**) EDF and (**b**) the RET framework.

As stated earlier, the heat generation is minimized when the variance of current dissipation over time is minimized. Note that this is performed alternatively by minimizing the sum of current consumption as revealed in lines 14–19 of Algorithm 2. In the originally given trace $I[t]$, the variance over time can be calculated as follows:

$$Var(I[t]) = \frac{\sum_{k=0}^{N}(I[k] - avg)^2}{N+1} \tag{4}$$

in which avg and N denote the average current dissipation and the maximum time stamp, respectively. By scheduling τ_i^j from m, the variance is changed to

$$Var(I'[t]) = \frac{\sum_{k=0}^{N}(I[k] + b_i^j[k] \cdot P_i^j - avg')^2}{N+1} \tag{5}$$

in which avg' denotes the changed average current dissipation and $b_i^j[k]$ denotes a binary variable that is only 1 if τ_i^j is in execution at time k. Note that avg' and P_i^j are not sensitive to the scheduling decision, i.e., $b_i^j[k]$. By developing $Var(I'[t]) - Var(I[t])$, it can be easily noticed that minimizing $Var(I'[t]) - Var(I[t])$ is equivalent to minimizing $\sum_{k=0}^{N}(b_i^j[k] \cdot P_i^j \cdot$

$I[k]$). Therefore, the minimization of $Var(I'[t])$ can be safely replaced with minimizing *temp* in line 15 of Algorithm 2.

4.3. Proposed On-Line Scheduling Policies

Based on empirical observations of the optimal temperature derived by Waldmann et al. [32], unlike the RET framework, we argue that the reduced heat generation is not beneficial to the battery lifetime in the satellite systems when they operate mostly at low temperatures. Hence, we take alternative approaches for the on-line scheduling decision. The first alternative, called MAX_VAR, is to find a starting time for each task with in its reserved time that simply maximizes the sum of current dissipation as shown in Figure 5a. In the example, the tasks are reserved in the order of τ_a^j, τ_a^i, τ_b^j, τ_b^i, and so forth. It can be seen that τ_a^i and τ_b^i are determined to be overlapped in time with τ_a^j and τ_b^j, respectively, to maximize the variance. However, this approach inevitably causes idle time slack post-fixed to the actual execution in most cases. Due to this, some chances of overlapping remain out of consideration. For example, as the second job of τ_a^j is scheduled at the beginning of its reserved time, the second job of τ_a^i will never be able to be executed at the same time with τ_a^j. To compensate for these lost possibilities of overlapping, we propose the second alternative, referred to as MAX_VAR_ALAP, which also searches for the starting time that maximizes the variance, but keeps the schedule as late as possible. As illustrated in Figure 5b, this approach allows τ_a^i and τ_a^j to be overlapped in time for their second jobs too.

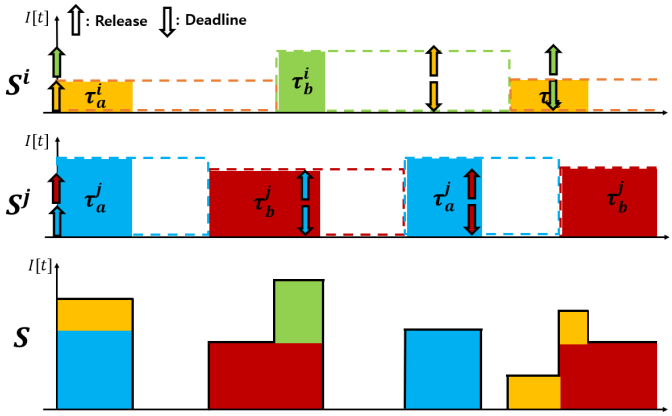

(**a**) A MAX_VAR scheduling example

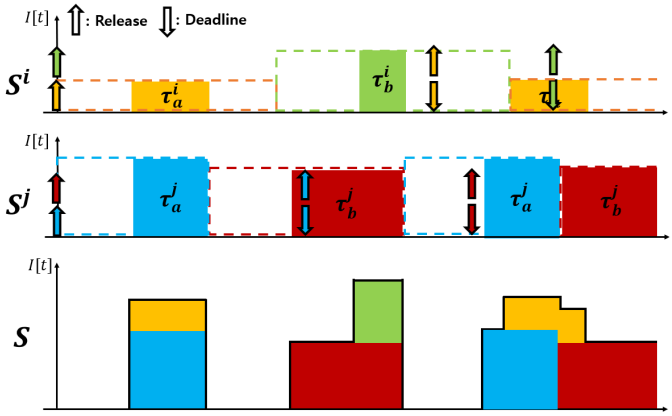

(**b**) A MAX_VAR_ALAP scheduling example

Figure 5. Examples of scheduling and current dissipation traces from the proposed on-line scheduling policies: (**a**) maximizing the variance (MAX_VAR) and (**b**) maximizing the variance while keeping the execution as late as possible (MAX_VAR_ALAP).

Algorithm 3 illustrates the on-line scheduling procedure of the MAX_VAR approach. The default scheduling decision is made in the same way as the RET policy using EDF. But, in determining the starting time of the reserved task, it considers the opposite objective; it searches for the starting time that results in the maximum variance. Note that the *max* value is initialized as 0, instead of $min \leftarrow \infty$ of the RET policy, as shown in line 13. Whenever a new maximum variance point is found (line 14), the starting time is updated (line 17).

Algorithm 3 Run time scheduling of the reserved tasks in the MAX_VAR approach

1: t_{now}: the current time step index
2: $I[t]$: current dissipation trace for $t \in [t_{now}, t_{max}]$
3: **if** a new task is reserved **then** ▷ By the default scheduling decision
4: $Q \leftarrow \phi$; ▷ Initialized ad an empty queue
5: **for** each $S^w \in S$ **do**
6: **if** S^w is reserved by τ_u^w and not in execution **then**
7: $enqueue(\tau_u^w)$ into Q;
8: **end if**
9: **end for**
10: Sort Q in a descending order of P_u^w; ▷ From more power-consuming ones to lesser
11: **while** $Q \neq \phi$ **do**
12: $\tau_u^w \leftarrow dequeue(Q)$;
13: $max \leftarrow 0; start \leftarrow t_{now}$;
14: **for** m in $[t_{now}, t_{now} + RV_u^w - X_u^w)$ **do**
15: $temp \leftarrow \sum_{t=m}^{m+X_u^w-1} \{I[t] + P_u^w\}$
16: **if** $temp > max$ **then**
17: $max \leftarrow temp; start \leftarrow m$;
18: **end if**
19: **end for**
20: **for** $i \in [start, start + X_u^w)$ **do** ▷ Update $I[t]$ as per the decided start time of τ_u^w
21: $I[i] \leftarrow I[i] + P_u^w$;
22: **end for**
23: **end while**
24: **end if**

Our goal in this on-line scheduling is to distribute the current dissipation workloads as unbalanced as possible. The calculated reserved time range safely keeps the scheduling decision free of any deadline violations. From the perspective of a single subsystem, one may think that it would be beneficial to place the task execution times consecutively by having horizontal execution bursts in Figure 5. However, as mathematically shown in the previous subsection, the variance is proportional to the sum of current dissipation of all subsystems over a certain period in time, i.e., the vertical bursts in Figure 5 matters. As exemplified in Figure 5, the MAX_VAR may result in sub-optimal scheduling in terms of vertical bursts by losing some possible overlaps.

In order to maximize the possibility of a task being overlapped with other tasks in other subsystem, we propose another alternative on-line scheduling, called MAX_VAR_ALAP,

that places the task execution as late as possible when the sums of current dissipation are tied for different starting points. For instance, the starting time of the second invocation of task τ_a^j in Figure 5b is scheduled at the end of its reserved time range, unlike the MAX_VAR approach. Afterwards, when the second invocation of τ_a^j is reserved, it can be overlapped in time with τ_a^j as shown in the figure. Algorithm 4 shows how the MAX_VAR_ALAP differ from the previous two on-line scheduling policies. Overall flow of the algorithm stays the same, but it searches for the maximum variance point in a reverse order. The starting index of the search loop (lines 14–20) is initialized to the latest possible starting point in the reserved time range, i.e., $t_{now} + RV_u^w - X_u^w - 1$, as shown in line 13 and the index of the loop is switched in an opposite order (line 19).

Algorithm 4 Run time scheduling of the reserved tasks in the MAX_VAR_ALAP approach

1: t_{now}: the current time step index
2: $I[t]$: current dissipation trace for $t \in [t_{now}, t_{max}]$
3: **if** a new task is reserved **then** ▷ By the default scheduling decision
4: $Q \leftarrow \phi$; ▷ Initialized ad an empty queue
5: **for** each $S^w \in S$ **do**
6: **if** S^w is reserved by τ_u^w and not in execution **then**
7: $enqueue(\tau_u^w)$ into Q;
8: **end if**
9: **end for**
10: Sort Q in a descending order of P_u^w; ▷ From more power-consuming ones to lesser
11: **while** $Q \neq \phi$ **do**
12: $\tau_u^w \leftarrow dequeue(Q)$;
13: $max \leftarrow 0$; $start \leftarrow t_{now} + RV_u^w - X_u^w - 1$; $m \leftarrow start$;
14: **while** $m \geq t_{now}$ **do**
15: $temp \leftarrow \sum_{t=m}^{m+X_u^w-1} \{I[t] + P_u^w\}$
16: **if** $temp > max$ **then**
17: $max \leftarrow temp$; $start \leftarrow m$;
18: **end if**
19: $m \leftarrow m - 1$;
20: **end while**
21: **for** $i \in [start, start + X_u^w)$ **do** ▷ Update $I[t]$ as per the decided start time of τ_u^w
22: $I[i] \leftarrow I[i] + P_u^w$;
23: **end for**
24: **end while**
25: **end if**

The time complexity of the proposed on-line scheduling policies, i.e., Algorithms 3 and 4, are identical to that of the RET approach (Algorithm 2) as $O(\max_{\tau_j^j \in \tau^j}(RV_i^j - X_i^j) \cdot n)$. It is worthwhile to mention that, unlike the offline procedure, the scheduling overhead of this on-line part can possibly affect the timing and current discharging behaviors. However,

in this work, we assume that this run time overhead is insignificant as in [6] and do not explicitly consider its effects both in timing and battery aging.

5. Evaluation

5.1. Battery Aging Simulator

The battery lifetime evaluation performed in the RET framework was based on the thermal-electrochemcial pseudo 2D battery model proposed by Bizeray et al. [29]. However, the open source simulator released by them only supports the calculation of the internal state for a single cycle. Thus, Kwak et al. [6] extended the simulator to support multiple cycles, based on the degradation model proposed by Jin et al. [23]. Unfortunately, the proposed technique cannot be directly evaluated with this simulator for two reasons. They adopted fairly simplified correlation models for the SEI growth and loss of active material. More importantly, they did not consider the lithium plating effect, which may be critical in the satellite environment.

For the evaluation of this work, we used the open-source Li-ion battery aging simulator , written in C++ and developed by Reiniers et al. [12], which is based on the same electrochemical model as Bizeray et al. [29] and considers the lithium plating effect. We made a couple of modifications to the simulator to make it compliant to the target system. First, we extended the simulator to have a variable ambient temperature. While the original implementation takes a constant room temperature, it has been customized to have varying environment temperature following Figure 1 as the simulation time proceeds. Second, the original simulator, which had the minimum time scale of 1 s, was also modified to work with a more sophisticated time scale (as small as 10 ms) as the minimum time scale we consider in the scheduling is 10 ms.

5.2. Simulation Setup

For satellite task workloads, we generated task sets using UUniFast-Discard algorithm [37], which can generate an uniformly distributed and unbiased task set for a given utilization. We assumed a number of satellite subsystems n is 4 and a number of tasks k in each subsystem is 5. Under this condition, we randomly generated a task set for each subsystem with four different utilization points, i.e., $U = \{0.2, 0.4, 0.6, 0.8\}$. For a single generated task, the period T_u^w was randomly selected within the range of [10, 1000] ms (with the minimum time unit being 10 ms) and the WCET X_u^w was decided to match with the given utilization with respect to the generated period, i.e., $\sum X_u^w / T_u^w$ should be equal to the utilization. The current dissipation P_u^w was randomly chosen within the range of $[0.01C, \frac{1}{U}C]$, where C is a measure of rate at which a battery is discharged relative to its maximum capacity. For instance, $2C$ denotes $2A$ for a battery whose maximum capacity is 1 Ah. These random task generation procedures were performed in MATLAB. The detailed information of the randomly generated task sets used for the simulation is summarized in Table 1.

The scale of current is a very important configuration in the estimation of battery lifetime as it is strongly related to heat generation. The RET framework considered the average current of $4C$ to be discharged in in their target systems, UAVs, in which a number power-consuming mechanical actuators exist. Considering the general amount of current requirements of the LEO battery cells [38], we set the average scale of discharge current and net charge current to $C/2$ and $C/3$ respectively. To reflect the real characteristics of satellite systems, we additionally consider the solar panel degradation with temperature increase. As the efficiency of power generation gradually decreases due to temperature rise [20], we reflect this degradation behavior modeled in [17] to the simulator. As stated in Section 2, the battery is also discharged when the demanding current is higher than the harvested current even during the sunlight period.

Table 1. Randomly generated task sets used for the battery lifetime simulations.

		Period					WCET					Current				
		T_1	T_2	T_3	T_4	T_5	T_1	T_2	T_3	T_4	T_5	T_1	T_2	T_3	T_4	T_5
$U = 0.2$	S^1	690	710	690	350	730	30	20	10	10	80	4.08	3.17	4.79	4.79	2.11
	S^2	130	780	250	140	380	10	20	10	10	30	4.53	0.49	4.83	2.43	4.58
	S^3	870	770	740	180	960	10	10	30	10	110	0.64	1.4	0.79	4.01	3.97
	S^4	940	450	120	840	130	20	30	10	10	10	4.57	2.74	4.86	0.71	4.8
$U = 0.4$	S^1	760	370	690	280	840	40	10	20	30	180	2.3	0.82	1.69	1.57	1.76
	S^2	410	120	870	970	420	20	10	10	30	110	0.74	0.24	0.28	0.94	0.99
	S^3	170	260	340	470	550	10	40	20	10	80	1.37	1.11	0.5	1.52	1.43
	S^4	370	880	910	300	780	60	70	50	10	80	1.96	0.08	1.33	2.12	0.63
$U = 0.6$	S^1	330	930	110	540	850	100	30	10	60	100	0.55	1.15	0.61	1.4	1.42
	S^2	800	190	760	410	250	140	20	100	10	40	1.33	0.09	0.94	0.3	1.35
	S^3	830	220	840	800	880	90	70	10	10	140	0.92	0.96	1.55	1.47	0.32
	S^4	550	880	200	350	940	130	20	20	50	90	0.39	1.66	0.44	0.47	1.64
$U = 0.8$	S^1	870	290	610	670	820	260	20	50	30	240	0.67	0.9	0.73	0.87	0.63
	S^2	100	380	840	150	240	20	30	50	30	60	1.17	0.61	0.98	0.5	0.08
	S^3	280	410	170	770	770	110	100	10	10	80	0.97	0.56	0.9	0.16	0.66
	S^4	900	820	270	640	780	30	160	50	120	150	0.51	1.18	0.18	0.81	0.4

In each simulation, we generated the current traces of 100 min for one single revolution period for four different scheduling policies: EDF, RET, MAX_VAR, and MAX_VAR_ALAP. For this, each scheduling algorithm was implemented in MATLAB. The scheduling was repeatedly performed with respect to the randomly generated task sets in MATLAB to obtain the current traces, which in turn were be fed into the battery aging simulator to evalute the battery lifetime. We have two baseline schedulers for comparison: EDF is the naive NP-EDF scheduler without any modification and RET denotes the scheduler proposed in [6]. Two proposed scheduling policies, MAX_VAR and MAX_VAR_ALAP are the ones described in Algorithms 3 and 4, respectively. Note that the generated current traces for the four different scheduling policies have the same average current dissipation, but with different variances. We feed the generated traces to the modified battery aging simulator in order to estimate the expected battery lifetimes. As the End Of Life (EOL) of battery is generally defined as the time taken to the moment at which the remaining battery capacity eventually reaches to 80% of its initial capacity [39], the simulation procedure should be repeated until the evaluated remaining capacity in the simulator reaches the 80% point. However, it is too burdensome to measure the remaining capacity every cycle. Thus, in favor of efficient simulation performance, we measured the remaining capacity every 100 cycles and linearly interpolated the variables between two consecutive measuring points. It is worthwhile to mention that the presented battery aging simulation is very time consuming. Advancing each cycle in the simulator requires a considerable computation power solving the differential equations in the model and the generated current traces consist of several hundreds of thousands time units to be evaluated. It takes approximately 45 h to complete the simulation of one generated task set on top of an Intel Core i7-10510U machine with 32 GB RAM running Windows 10. For the electro-chemical modeling of the satellite battery, we used the LG Chem NMC 18650 battery parameters reported in [40].

5.3. Simulation Results

Figure 6 illustrates the measured current variances and the simulated lifespans that four different scheduling policies result in for the four different randomly generated task sets. As shown in Figure 6a, the RET policy always causes the minimal current variance. On the other extreme, MAX_VAR_ALAP shows the highest current variances over the all four

cases. It increases the variance up to 238.73% from RET and up to 34.14% from EDF in the case of $U = 0.2$. These gaps gradually decrease as the utilization grows bigger (the degree of freedom in scheduling gets smaller). As analyzed with an example in Section 4.3, MAX_VAR could result in sub-optimal scheduling in terms of variance. This becomes evident when comparing the measured variances of MAX_VAR and MAX_VAR_ALAP. It sometimes results in even smaller variance than EDF and this implies that the slacks caused by the reserved time may work against the prolonged battery lifetime.

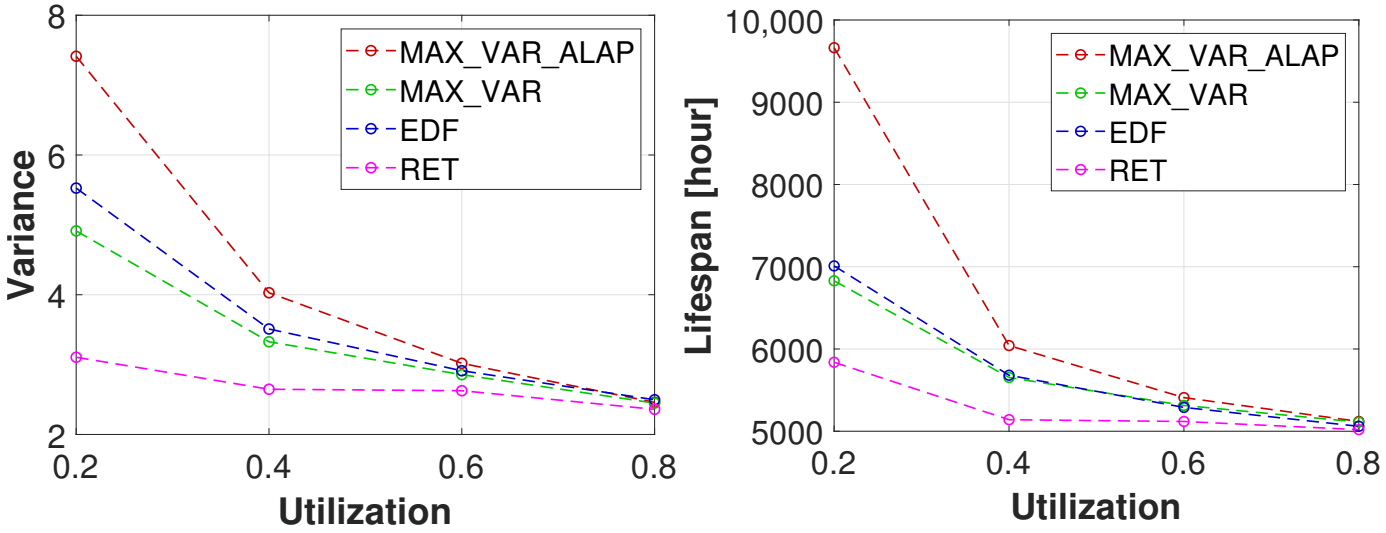

(**a**) Measured current variances

(**b**) Simulated lifespans

Figure 6. Simulation results of different scheduling policies.

The simulated lifespans reported in Figure 6b show the same tendency as the variance. Comparing the lifetime caused by MAX_VAR_ALAP with that of RET, an improvement of 65.51% is achieved in the case of $U = 0.2$. For the other utilization points, $U = 0.4, 0.6, 0.8$, the expected lifespan gain are lesser, 17.54%, 5.67%, and 1.99%, respectively, as the degree of freedom in scheduling diminishes. This results prove that, on the contrary to the conclusion of the RET framework [6], the increased current variances can actually extend the lifespan of batteries in the satellite systems. This anomaly is attributed to the fact that the heat generation due to such increased variance can mitigate the lithium plating effect for satellite systems when they operate in low temperatures. Note that other aging effects may be accelerated in this case. This results can be verified in the battery cell temperature profile obtained by the simulator. The internal cell temperature profile reported by the simulator for the case of $U = 0.2$ is illustrated in Figure 7. As expected, MAX_VAR_ALAP always generates more heat than other policies and the the RET policy shows the lowest temperature throughout the entire revolution period. The minimum cell temperature was observed to be 3.35 °C when the tasks are scheduled by the MAX_VAR_ALAP policy, while it was 2.45 °C for the RET policy.

As a result of the temperature difference, it has been observed that MAX_VAR_ALAP promotes the amount of SEI layer by up to 13.10% (compared with RET), while the lithium plating effect in RET is promoted by 230.78% in the case of $U = 0.2$. In summary, the existing strategy that focuses on minimizing the heat generation can result in a serious adverse effect in the battery lifetime when the system operates in considerably low temperatures. The same tendency has been observed in the comparison between MAX_VAR_ALAP and EDF. In case of $U = 0.2, 0.4, 0.6$, the lifespan extension by MAX_VAR_ALAP are 37.85%, 6.35%, and 2.23%, respectively.

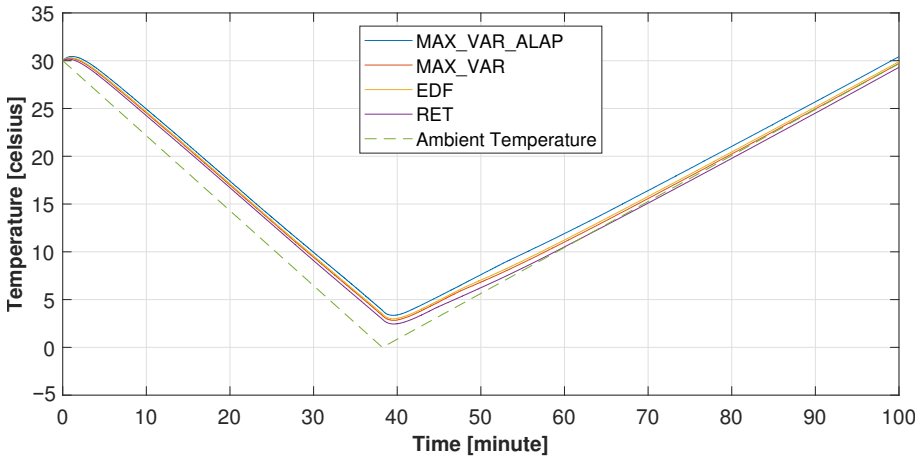

Figure 7. Simulated battery internal cell temperature profile at for $U = 0.2$.

5.4. Discussion and Future Work

For embedded systems, it is known that the choice of scheduling may influence a number of system behaviors, e.g., energy consumption, performance, and dependability of real-time control systems, and so forth. In particular, since the proposed method includes an online part as stated in Section 4.3, it can possibly cause non-negligible effects in timing and power consumption in large systems. Therefore, it is necessary to further investigate how the scheduling overhead affects the system.

Since the Li-ion battery is associated with non-linear factors, such as rate capacity effect, a fluctuating discharge current can cause a reduced discharge efficiency [41]. It has been known that LEO satellites generally keep the DOD shallow, as small as about 10%–40% [38], as it can be a dominantly contributing factor to lifespan degradation [42].This implies that a current trace generated by the variance-maximizing policy, like the proposed one, may result in this inefficiency. Thus, more quantitative analysis and optimization will be needed to perform to determine the best degree of distributed current workloads with respect to a given pair of temperature and DOD condition. Also, the battery power capability, which is usually limited under low temperature, can be increased by the generated heat from unbalanced current dissipation. In fact, it is possible to further optimize the trade-off between the usable battery capacity in a cycle and the lifetime. We leave this co-optimization as a future work.

Furthermore, it is noteworthy that the proposed scheduling policy is simply built upon an empirical observation that the increased battery temperature always results in better lifetime, thanks to the mitigation of the lithium plating effect. While this assumption holds true for the tested simulation setup, the optimal temperature, in principle, may vary depending on the battery cell characteristics. This implies that a more general adaptive scheduling policy can be developed to keep the temperature close to optimal one if the optimal temperature can be analyzed in advance. Such an adaptive scheduling approach could also be effective to handle uncertain workloads, e.g., event-driven workloads such as communications with ground stations. This also remains as a future research topic.

6. Conclusions

In this paper, we deal with a real-time scheduling technique that lengthens the Li-ion battery lifetime in satellite systems. We showed that the existing scheduling policy, which was proposed to minimize the heat dissipation, may cause even reduced battery lifetime for the target satellite systems. This anomaly is attributed to the fact that the existing scheduling policy assumed a fixed normal ambient temperature and did not take the lithium plating effect into consideration in estimating battery lifetime for satellite systems operating in low temperature. Hence, we proposed an alternative battery-aware scheduling policy which better suits to the LEO satellite systems. In the alternative scheduling policies we proposed, the current discharge loads are placed as unbalanced as possible with respect

to the real-time constraints, in favor of increased temperature by scheduling, to mitigate the lithium plating effect. The simulation results performed on a modified open-source simulator proved that the proposed scheduling could considerably enhance the expected lifetime by up to 65.51%.

Author Contributions: Conceptualization, S.J. and H.Y.; methodology, S.J. and H.Y.; software, S.J.; validation, S.J.; writing—original draft preparation, S.J. and H.Y; writing—review and editing, S.J. and H.Y.; visualization, S.J.; supervision, H.Y.; project administration, H.Y.; funding acquisition, H.Y. Both authors have read and agreed to the published version of the manuscript.

Funding: This research was supported by the MSIT (Ministry of Science and ICT), Korea, under the ITRC (Information Technology Research Center) support program (IITP-2021-2018-0-01424) supervised by the IITP (Institute for Information & communications Technology Promotion).

Institutional Review Board Statement: Not applicable.

Informed Consent Statement: Not applicable.

Data Availability Statement: The data presented in this study are available in the article.

Conflicts of Interest: The authors declare no conflict of interest. The funder had no role in the design of the study; in the collection, analyses, or interpretation of data; in the writing of the manuscript, or in the decision to publish the results.

Abbreviations

The following abbreviations are used in this manuscript:

Li-ion	Lihtium-ion
EV	Electric Vehicles
UAV	Unmanned Aerial Vehicles
LEO	Low Earth Orbit
DOD	Depth Of Discharge
SOC	State Of Charge
RET	Reserved Execution Time
WCET	Worst Case Execution Time
SEI	Solid Electroyte Interface
EDF	Earliest Deadline First
NP-EDF	Non Preemptive Earliest Deadline First
EOL	End Of Life

References

1. Armand, M.; Tarascon, J.M. Building better batteries. *Nature* **2008**, *451*, 652–657. [CrossRef] [PubMed]
2. Tsuchida, H.; Kawamoto, Y.; Kato, N.; Kaneko, K.; Tani, S.; Uchida, S.; Aruga, H. Efficient Power Control for Satellite-Borne Batteries Using Q-Learning in Low-Earth-Orbit Satellite Constellations. *IEEE Wirel. Commun. Lett.* **2020**, *9*, 809–812. [CrossRef]
3. Lami, M.; Shamayleh, A.; Mukhopadhyay, S. Minimizing the state of health degradation of Li-ion batteries onboard low earth orbit satellites. *Soft Comput.* **2020**, *24*, 4131–4147. [CrossRef]
4. Chon, Y.; Lee, G.; Ha, R.; Cha, H. Crowdsensing-based smartphone use guide for battery life extension. In Proceedings of the 2016 ACM International Joint Conference on Pervasive and Ubiquitous Computing, Heidelberg, Germany, 12–16 September 2016; pp. 958–969.
5. Wegmann, R.; Döge, V.; Sauer, D.U. Assessing the potential of a hybrid battery system to reduce battery aging in an electric vehicle by studying the cycle life of a graphite| NCA high energy and a LTO| metal oxide high power battery cell considering realistic test profiles. *Appl. Energy* **2018**, *226*, 197–212. [CrossRef]
6. Kwak, J.; Lee, K.; Kim, T.; Lee, J.; Shin, I. Battery Aging Deceleration for Power-Consuming Real-Time Systems. In Proceedings of the 2019 IEEE Real-Time Systems Symposium (RTSS), Hong Kong, China, 3–6 December 2019; pp. 353–365.
7. Barré, A.; Deguilhem, B.; Grolleau, S.; Gérard, M.; Suard, F.; Riu, D. A review on lithium-ion battery ageing mechanisms and estimations for automotive applications. *J. Power Sources* **2013**, *241*, 680–689. [CrossRef]
8. Yang, X.G.; Wang, C.Y. Understanding the trilemma of fast charging, energy density and cycle life of lithium-ion batteries. *J. Power Sources* **2018**, *402*, 489–498. [CrossRef]
9. Alipour, M.; Ziebert, C.; Conte, F.V.; Kizilel, R. A review on temperature-dependent electrochemical properties, aging, and performance of lithium-ion cells. *Batteries* **2020**, *6*, 35. [CrossRef]

10. Wu, Y.; Keil, P.; Schuster, S.F.; Jossen, A. Impact of temperature and discharge rate on the aging of a LiCoO2/LiNi0. 8Co0. 15Al0. 05O2 lithium-ion pouch cell. *J. Electrochem. Soc.* **2017**, *164*, A1438. [CrossRef]
11. Wu, W.; Wu, W.; Qiu, X.; Wang, S. Low-temperature reversible capacity loss and aging mechanism in lithium-ion batteries for different discharge profiles. *Int. J. Energy Res.* **2019**, *43*, 243–253. [CrossRef]
12. Reniers, J.M.; Mulder, G.; Howey, D.A. Review and performance comparison of mechanical-chemical degradation models for lithium-ion batteries. *J. Electrochem. Soc.* **2019**, *166*, A3189. [CrossRef]
13. Sciotti, M.; Besso, P.; Flohrer, T.; Krag, H. Low Earth Orbit objects tracking and orbit determination from ground-based phased array radar systems. In Proceedings of the 2011 12th International Radar Symposium (IRS), Leipzig, Germany, 7–9 September 2011; pp. 591–596.
14. Guo, R.; Lu, L.; Ouyang, M.; Feng, X. Mechanism of the entire overdischarge process and overdischarge-induced internal short circuit in lithium-ion batteries. *Sci. Rep.* **2016**, *6*, 30248. [CrossRef] [PubMed]
15. Belov, D.; Yang, M.H. Failure mechanism of Li-ion battery at overcharge conditions. *J. Solid State Electrochem.* **2008**, *12*, 885–894. [CrossRef]
16. Qi, J.; Lu, D.D.C. Review of battery cell balancing techniques. In Proceedings of the 2014 Australasian Universities Power Engineering Conference (AUPEC), Perth, WA, Australia, 28 September–1 October 2014; pp. 1–6.
17. Lee, J.; Kim, E.; Shin, K.G. Design and management of satellite power systems. In Proceedings of the 2013 IEEE 34th Real-Time Systems Symposium, Vancouver, BC, Canada, 3–6 December 2013; pp. 97–106.
18. Mostacciuolo, E.; Vasca, F.; Baccari, S.; Iannelli, L.; Sagnelli, S.; Luisi, R.; Stanzione, V. An optimization strategy for battery charging in small satellites. In Proceedings of the 2019 European Space Power Conference (ESPC), Juan-les-Pins, France, 30 September–4 October 2019; pp. 1–8.
19. Mostacciuolo, E.; Iannelli, L.; Sagnelli, S.; Vasca, F.; Luisi, R.; Stanzione, V. Modeling and power management of a LEO small satellite electrical power system. In Proceedings of the 2018 European Control Conference (ECC), Limassol, Cyprus, 12–15 June 2018; pp. 2738–2743.
20. Jordan, F. SwissCube: Electrical Power System, Final Report. Available online: http://www.goldstem.org/Swiss%20Cube/03%20-%20Power%20systems/S3-A-EPS-1-0-EPS.pdf (accessed on 30 December 2020).
21. Peterson, S.B.; Apt, J.; Whitacre, J. Lithium-ion battery cell degradation resulting from realistic vehicle and vehicle-to-grid utilization. *J. Power Sources* **2010**, *195*, 2385–2392. [CrossRef]
22. Schimpe, M.; von Kuepach, M.E.; Naumann, M.; Hesse, H.C.; Smith, K.; Jossen, A. Comprehensive modeling of temperature-dependent degradation mechanisms in lithium iron phosphate batteries. *J. Electrochem. Soc.* **2018**, *165*, A181. [CrossRef]
23. Jin, X.; Vora, A.; Hoshing, V.; Saha, T.; Shaver, G.; García, R.E.; Wasynczuk, O.; Varigonda, S. Physically-based reduced-order capacity loss model for graphite anodes in Li-ion battery cells. *J. Power Sources* **2017**, *342*, 750–761. [CrossRef]
24. Delacourt, C.; Safari, M. Life simulation of a graphite/LiFePO4 cell under cycling and storage. *J. Electrochem. Soc.* **2012**, *159*, A1283. [CrossRef]
25. Safari, M.; Delacourt, C. Simulation-based analysis of aging phenomena in a commercial graphite/LiFePO4 cell. *J. Electrochem. Soc.* **2011**, *158*, A1436. [CrossRef]
26. Rao, R.; Vrudhula, S.; Rakhmatov, D.N. Battery modeling for energy aware system design. *Computer* **2003**, *36*, 77–87.
27. Zhang, Y.; Xiong, R.; He, H.; Qu, X.; Pecht, M. State of charge-dependent aging mechanisms in graphite/Li (NiCoAl) O2 cells: Capacity loss modeling and remaining useful life prediction. *Appl. Energy* **2019**, *255*, 113818. [CrossRef]
28. Shi, Q.; Liu, W.; Qu, Q.; Gao, T.; Wang, Y.; Liu, G.; Battaglia, V.S.; Zheng, H. Robust solid/electrolyte interphase on graphite anode to suppress lithium inventory loss in lithium-ion batteries. *Carbon* **2017**, *111*, 291–298. [CrossRef]
29. Bizeray, A.M.; Zhao, S.; Duncan, S.R.; Howey, D.A. Lithium-ion battery thermal-electrochemical model-based state estimation using orthogonal collocation and a modified extended Kalman filter. *J. Power Sources* **2015**, *296*, 400–412. [CrossRef]
30. Waldmann, T.; Hogg, B.I.; Kasper, M.; Grolleau, S.; Couceiro, C.G.; Trad, K.; Matadi, B.P.; Wohlfahrt-Mehrens, M. Interplay of operational parameters on lithium deposition in lithium-ion cells: Systematic measurements with reconstructed 3-electrode pouch full cells. *J. Electrochem. Soc.* **2016**, *163*, A1232. [CrossRef]
31. Liaw, B.Y.; Roth, E.P.; Jungst, R.G.; Nagasubramanian, G.; Case, H.L.; Doughty, D.H. Correlation of Arrhenius behaviors in power and capacity fades with cell impedance and heat generation in cylindrical lithium-ion cells. *J. Power Sources* **2003**, *119*, 874–886. [CrossRef]
32. Waldmann, T.; Wilka, M.; Kasper, M.; Fleischhammer, M.; Wohlfahrt-Mehrens, M. Temperature dependent ageing mechanisms in Lithium-ion batteries–A Post-Mortem study. *J. Power Sources* **2014**, *262*, 129–135. [CrossRef]
33. Poghosyan, A.; Golkar, A. CubeSat evolution: Analyzing CubeSat capabilities for conducting science missions. *Prog. Aerosp. Sci.* **2017**, *88*, 59–83. [CrossRef]
34. Weston, S.; Miller, C.S.; Ingersoll, J.E.; Yost, B.D.; Agasid, E.; Burton, R.; Carlino, R.; Defouw, G.; Perez, A.D.; Karacalioglu, A.G.; et al. State of the Art: Small Spacecraft Technology. Available online: https://ntrs.nasa.gov/citations/20200001421 (accessed on 30 December 2020).
35. Boushon, K.E. Thermal Analysis and Control of Small Satellites in Low Earth Orbit. Master's Thesis, Missouri University of Science and Technology, Rolla, MO, USA, 2018.
36. Jeffay, K.; Stanat, D.F.; Martel, C.U. On non-preemptive scheduling of periodic and sporadic tasks. In Proceedings of the Twelfth IEEE Real-Time Systems Symposium, San Antonio, TX, USA, 4–6 December 1991; pp. 129–139.

37. Davis, R.I.; Burns, A. Priority assignment for global fixed priority pre-emptive scheduling in multiprocessor real-time systems. In Proceedings of the 2009 30th IEEE Real-Time Systems Symposium, Washington, DC, USA, 1–4 December 2009; pp. 398–409.
38. Borthomieu, Y. Satellite Lithium-ion batteries. In *Lithium-Ion Batteries*; Elsevier: Amsterdam, The Netherlands, 2014; pp. 311–344.
39. Palacín, M.R. Understanding ageing in Li-ion batteries: A chemical issue. *Chem. Soc. Rev.* **2018**, *47*, 4924–4933. [CrossRef]
40. Chem, L. Rechargeable Lithium Ion Battery Model: INR18650 MJ1 3500 mAh. Available online: https://www.nkon.nl/sk/k/Specification%20INR18650MJ1%2022.08.2014.pdf (accessed on 30 December 2020).
41. Shin, D.; Kim, Y.; Seo, J.; Chang, N.; Wang, Y.; Pedram, M. Battery-supercapacitor hybrid system for high-rate pulsed load applications. In Proceedings of the 2011 Design, Automation & Test in Europe, Grenoble, France, 14–18 March 2011; pp. 1–4.
42. He, G.; Chen, Q.; Kang, C.; Pinson, P.; Xia, Q. Optimal bidding strategy of battery storage in power markets considering performance-based regulation and battery cycle life. *IEEE Trans. Smart Grid* **2015**, *7*, 2359–2367. [CrossRef]